Biosensors and Bioelectronics 43 (2013) 308–314

Contents lists available at SciVerse ScienceDirect

Biosensors and Bioelectronics

journal homepage: www.elsevier.com/locate/bios

Design of label-free, homogeneous biosensing platform based on plasmonic coupling and surface-enhanced Raman scattering using unmodified gold nanoparticles

Zi Yi, Xiao-Yan Li, Feng-Juan Liu, Pei-Yan Jin, Xia Chu*, Ru-Qin Yu

State Key Laboratory of Chemo/Bio-Sensing and Chemometrics, College of Chemistry and Chemical Engineering, Hunan University, Changsha 410082, PR China

ARTICLE INFO

Article history:
Received 1 September 2012
Received in revised form
22 November 2012
Accepted 4 December 2012
Available online 13 December 2012

Keywords:
Surface-enhanced Raman scattering
Gold nanoparticle
Raman active dye
Biosensor

ABSTRACT

Surface-enhanced Raman scattering (SERS) has emerged as a promising spectroscopic technique for biosensing. However, to design a SERS-based biosensor, almost all currently used methods involve the time-consuming and complicated modification of the metallic nanoparticles with the Raman active dye and biorecognition element, which restricts their widespread applications. Herein, we report a label-free, homogeneous and easy-to-operate biosensing platform for the rapid, simple and sensitive SERS detection by using the unmodified gold nanoparticles (Au NPs). This strategy utilizes the difference in adsorption property of single-stranded DNA (ssDNA) and double-stranded DNA (dsDNA) on citrate-coated Au NPs. In the presence of dsDNA, the aggregation of Au NPs takes place after adding salt solution because the dsDNA cannot adsorb on the Au NPs to protect them from salt-induced aggregation. Such aggregation gives rise to the plasmonic coupling of adjacent metallic NPs and turns on the enhancement of the Raman scattering, displaying a strong SERS signal. In contrast, the ssDNA can adsorb on the Au NPs surface through strong electrostatic attraction and protect them from salt-induced aggregation, showing a weak SERS signal. This approach is not only straightforward and simple in design but also rapid and convenient in operation. The feasibility and universality of the design have been demonstrated successfully by the detection of DNA and Hg^{2+}, and the assay possesses the superior signal-to-background ratio as high as ~30 and excellent selectivity. The method can be extended to detect various analytes, such as other metal ions, proteins and small molecules by using the oligonucleotides that can selectively bind the analytes.

© 2012 Elsevier B.V. All rights reserved.

1. Introduction

Surface-enhanced Raman scattering (SERS) has emerged as a promising spectroscopic technique for biosensing because of its unique advantages, including high sensitivity with a potential of single molecule detection, highly informative spectra characteristics of molecules, multiplexed detection capability with a single laser excitation resulting from the narrow line width of Raman bands, as well as easy operation without complicated sample preparation (Campion and Kambhampati, 1998; Nie and Emory, 1997; Wang et al., 2003). Many studies have successfully demonstrated the great potential of SERS as an efficient biosensing platform, and, up to now, SERS has been widely employed for the detection of various biomolecules, including peptides (Herne et al., 1991; Mitchell et al., 2008), proteins (Han et al., 2008, 2009a, 2009b; He et al., 2011; Kahraman et al., 2010), DNA and RNA (Cao et al., 2002; Braun et al., 2007; Lierop et al., 2011; Lowe et al., 2010), bacteria (Yang et al., 2011; Jarvis et al., 2004; Preciado-Flores et al., 2011), and living cells (Ock et al., 2012; Tang et al., 2008; Zong et al., 2011).

To design a SERS-based biosensor, the most common strategy normally utilizes the so-called SERS tags with both the SERS-activity and the biorecognition function. Typically, these tags are prepared by direct attachment of Raman reporter molecules and biorecognition elements to the surface of silver/gold metallic nanoparticles or by sandwiching the Raman reporter molecules between a metallic nanoparticle core and a thin silica shell, on which the biorecognition elements are immobilized. The biosensing is then performed in a sandwich immunoassay or a sandwich DNA hybridization assay format on a solid substrate. Although this strategy has been successfully applied to the detection of small molecule (Li et al., 2012), protein (Wang et al., 2011; Schmit et al., 2012; Hwang et al., 2010; Chon et al., 2010), nucleic acid (Zhang et al., 2011) and even to the bioimaging of living cells (Qian et al.,

* Corresponding author. Tel./fax: +86 731 88821916.
E-mail addresses: xiachu@hnu.cn, xiachu@hnu.edu.cn, xiachu1972@yahoo.com.cn (X. Chu).

0956-5663/$ - see front matter © 2012 Elsevier B.V. All rights reserved.
http://dx.doi.org/10.1016/j.bios.2012.12.002

2008a; Liu et al., 2010), the time-consuming and complicated preparation of the SERS tags and the cumbersome, multi-step washing process make it challenging to carry out direct, label-free SERS detection. Recent studies have revealed that the SERS signals can be controlled and modulated by electromagnetic field enhancement in interparticle plasmon coupling (Hao and Schatz, 2004; Michaels et al., 1999), which offers a new strategy to design SERS-based biosensors through the controlled assembly of metallic nanoparticles to turn on the enhancement of the Raman scattering in a homogeneous solution. Several approaches have been investigated in an attempt to realize this strategy such as the detection of DNA through the controlled assembly of Raman active dye-coded gold/silver nanoparticles by DNA hybridization (Graham et al., 2008; Qian et al., 2008b), pH detection through the molecular conformation change of the thiolated block copolymer-functionalized gold nanoparticles (Qian et al., 2009), and protein detection through the controlled assembly by specific protein–ligand interactions (Han et al., 2010). However, all of these approaches still involve the preparation of the Raman active dye and biorecognition element-labeled metallic nanoparticles, which restricts their widespread applications. So, the development of a label-free, homogeneous biosensing strategy for the rapid, simple and sensitive SERS detection has remained highly desired.

Recent studies have found that single-stranded oligonucleotide (ssDNA) can adsorb to the citrate-coated gold nanoparticles (Au NPs) through attractive electrostatic interactions between the exposed bases and the Au NPs, which prevents the Au NPs from salt-induced aggregation, but the double-stranded oligonucleotide (dsDNA) does not because dsDNA has a stable double-helix geometry that always presents the negatively charged phosphate backbone (Li and Rothberg, 2004a). By taking advantage of this observation, many label-free colorimetric methods based on unmodified Au NPs have been developed for the detection of nucleic acid (Li and Rothberg, 2004b; Xin et al., 2009), protein (Wei et al., 2007), small molecules (Zhang et al., 2008) and metal ions (Lee et al., 2008; Wang et al., 2008a, 2008b). However, all of these methods have been prompted by changes in the color of Au NPs after aggregation, and, to the best of our knowledge, no studies has been reported based on the surface-enhanced Raman scattering. We reason that, if Raman reporter molecules are adsorbed to the surface of Au NPs, the aggregation of Au NPs might give rise to the plasmonic coupling of adjacent metallic NPs and turn on the enhancement of the Raman scattering. On the basis of this hypothesis, we develop a label-free, homogeneous biosensing platform for the rapid, simple and sensitive SERS detection. Different from the methods previously reported (Graham et al., 2008; Qian et al., 2008b, 2009; Han et al., 2010), which need the covalent modification of the metallic nanoparticles with the Raman active dye and biorecognition element, our proposed strategy employs unmodified Au NPs, which circumvents the time-consuming and complicated covalent modification process of metallic nanoparticles and significantly simplifies the procedure of SERS detection. In addition, compared with the colorimetric methods, the SERS-based detection can afford increased signal-to-background ratio and avoid endogenous color interferences from the target analyte. Combining these unique features, the developed strategy can provide a label-free, homogeneous and easy-to-operate biosensing platform for the rapid, simple and sensitive SERS detection.

2. Experimental

2.1. Materials and apparatus

All oligonucleotides used in this work were synthesized by Takara Biotechnology Co. Ltd. (Dalian, China). The sequences of the oligonucleotides were given in Table S1 of Supplementary Materials. All oligonucleotides were dissolved in highly pure water as stock solution, and the concentrations of the solution were estimated by UV absorption using published sequence-dependent absorption coefficients (Cantor et al., 1970). Hydrogen tetrachloroaurate (III) ($HAuCl_4 \cdot 4H_2O$), Mops ($C_7H_{14}NO_4SNa$) and sodium citrate ($C_6H_5Na_3O_7$) were all purchased from Sigma–Aldrich Chemical Co. Crystal violet was purchased from Tianjin Kermel Chemical Reagent Co., Ltd. (Tianjin, China). All solutions were prepared using ultrapure water, which was obtained through a Millipore Milli-Q water purification system (Billerica, MA) and had an electrical resistance of >18.3 MΩ.

SERS spectra were recorded on a Confocal Raman System Laboram 010 (Jobin Yvon Horiba, France) based on a 50× long working-distance objective. A 632.8 nm laser excitation (5 mW) was used. The integration time was 10 s. UV–vis absorption spectra were recorded in 1 cm path length quartz cuvettes on a Shimadzu UV-2450 UV–vis spectrophotometer (Kyoto, Japan). Transmission electron microscopy (TEM) was used to characterize the sizes of the monodispersed gold nanoparticles (Au NPs) and the Au NP aggregates. The samples were prepared by dropping the sample solution (4 μL) onto a carbon-coated copper grid. The solution was wicked from the edge of the grid with a piece of filter paper after 1 min and then dried naturally in air. Transmission electron microscopy images were taken with a Hitachi TEM 800 (Tokyo, Japan).

2.2. Synthesis of Au NPs

Citrate-coated Au NPs were prepared by citrate reduction of $HAuCl_4$ according to documented protocols (Ray, 2006; Darbha et al., 2008; Griffin et al., 2009), as briefly described as follows: trisodium citrate (2.3 mL, 1%) was added rapidly to a stirred boiling solution of $HAuCl_4$ (100 mL, 0.02%). Within several minutes, the color of the solution changed from pale yellow to deep red. The solution was heated under reflux for another 30 min to ensure complete reduction, and it was then slowly cooled to room temperature and stored at 4 °C before use. The average size of the Au NPs was 30 ± 5 nm in diameter as determined from the TEM image. The concentration of Au NPs was calculated to be about 5.3×10^{-10} M based on a molar extinction coefficient of $3.0 \times 10^9\ M^{-1}\ cm^{-1}$ at 530 nm for 30 nm Au NPs (Ray, 2006; Darbha et al., 2008; Griffin et al., 2009). The colloidal solutions of Au NP with different sizes were synthesized in a similar manner by adjusting the concentration of sodium citrate using the protocols reported previously (Ray, 2006; Darbha et al., 2008; Griffin et al., 2009).

2.3. SERS-based detection of DNA

A mixture solution containing varying concentrations of DNA target, 3 μM DNA probe, 0.1 M phosphate buffer (pH 7.4) and 100 mM NaCl (the total volume was 10 μL) was first incubated at 37 °C for 1 h. Subsequently, 50 μL of Au NPs colloidal solution, 20 μL of H_2O and 10 μL of 1 μM crystal violet were added into the mixture solution and then incubated at room temperature for 30 min. Finally, 10 μL of 250 mM NaCl solution was added into the mixture (the total volume was 100 μL). The SERS and UV–vis absorption spectra of the mixture were then recorded.

2.4. SERS-based detection of Hg^{2+}

For Hg^{2+} detection, 50 μL of Au NPs colloidal solution, 14 μL of H_2O, 5 μL of Mops buffer (0.2 M, pH 7.4), 3 μL of 10 μM Hg^{2+} probe, 10 μL of 1 μM crystal violet, and 4 μL of varying concentrations of Hg^{2+} solution (or other metallic ions) were mixed and

incubated at room temperature for 30 min. After adding 14 μL of 250 mM NaCl solution (the total volume was 100 μL), the SERS and UV–vis absorption spectra of the mixture were then recorded.

3. Results and discussion

3.1. Sensing principle of SERS-based detection

Our proposed strategy for SERS detection using unmodified Au NPs is shown in Scheme 1. The important insights in the strategy are mainly based on the following: (1) there are differences in adsorption properties of ssDNA and dsDNA on citrate-coated Au NPs. The ssDNA adsorbs efficiently on the Au NPs surface through strong electrostatic attraction while dsDNA does not, which results in ssDNA that can protect the Au NPs from salt-induced aggregation, but dsDNA cannot. (2) the aggregation of monodispersed Au NPs into discrete clusters can give rise to the plasmonic coupling and the formation of many SERS "hot spots", resulting in the enormous enhancement of Raman scattering. To test the general feasibility of the approach, the detection of DNA is first performed. As illustrated in Scheme 1, when the target DNA is complementary to the probe DNA, a double-stranded structure is formed. After the addition of unmodified Au NPs, Raman reporter molecules and NaCl, the aggregation of Au NPs occurs due to lack of the protection of ssDNA, resulting in a strong SERS signal. On the contrary, when the target DNA is not complementary to the probe DNA, the hybridization does not take place. The ssDNA adsorbs on the Au NPs surface and protects Au NPs from salt-induced aggregation, leading to a weak SERS signal. This approach is not only straightforward and simple in design but also fairly rapid and convenient in operation. To our knowledge, this is the first example of SERS-based DNA detection through the aggregation of unmodified Au NPs.

The Raman enhancement effect of the monodispersed Au NPs after the salt-induced aggregation was first investigated. Crystal violet (CV) was selected as the Raman reporter molecule because of its distinct Raman signatures and electrostatic attraction with the citrate-coated Au NPs. As shown in Fig. 1A, the citrate-coated Au NPs adsorbed with CV gave a very weak SERS signal (curve a). Also, a well-defined surface plasmon resonance peak at 530 nm shown in Fig. 1B (curve a) demonstrated that the addition of a certain amount of CV did not result in the appreciable aggregation of Au NPs. However, after adding the NaCl solution, a substantial increase in the SERS intensity can be observed (curve b of Fig. 1A), accompanied with an obvious red-to-purple color change as well

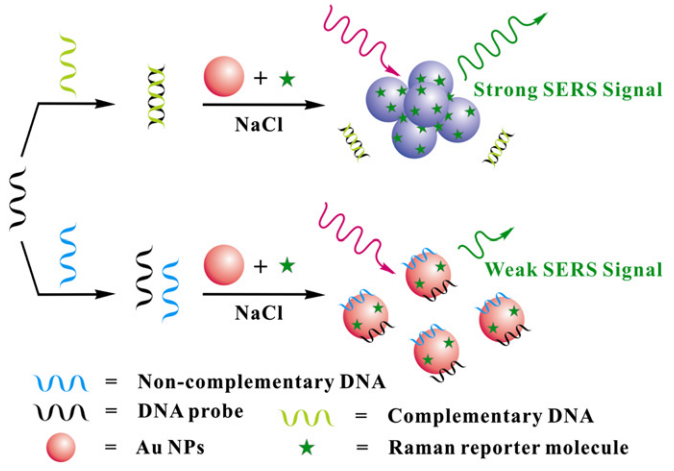

Scheme 1. Design scheme of the label-free, homogeneous, SERS-based biosensing platform for the detection of DNA using unmodified gold nanoparticles.

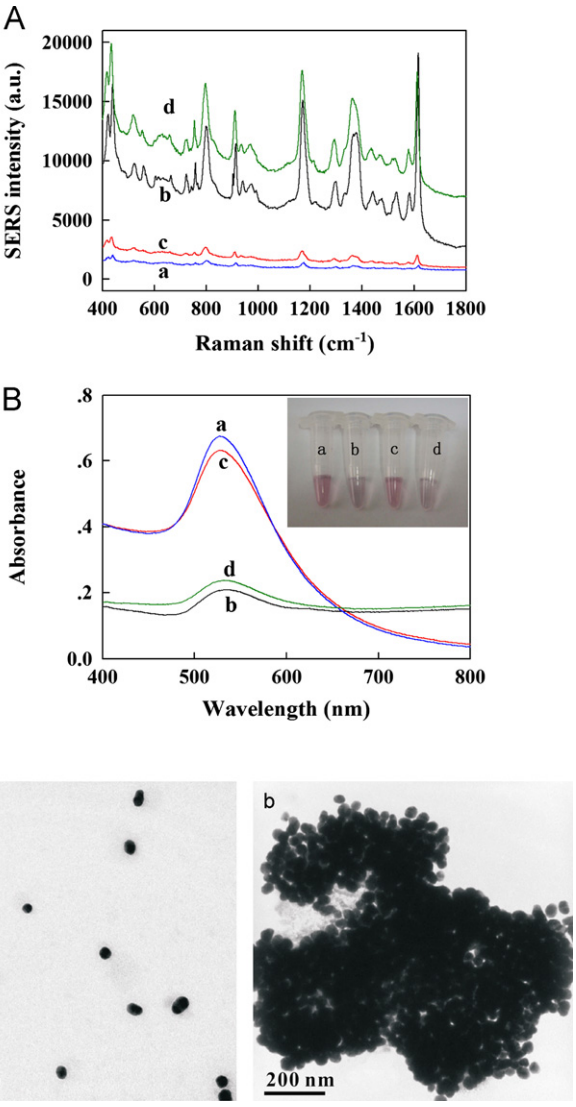

Fig. 1. SERS (A) and absorption (B) spectra obtained under different conditions: (a) Au NPs+CV, (b) Au NPs+CV+NaCl, (c) DNA probe+non-complementary DNA target+Au NPs+CV+NaCl, and (d) DNA probe+complementary DNA target+Au NPs+CV+NaCl. The inset is the photograph for the corresponding systems. (C) TEM images obtained under different conditions: (a) DNA probe+non-complementary DNA target+Au NPs+CV+NaCl, and (b) DNA probe+complementary DNA target+Au NPs+CV+NaCl. (For interpretation of the references to color in this figure caption, the reader is referred to the web version of this article.)

as significant broadening and red shifting of the absorption spectrum (curve b of Fig. 1B). These results indicate that the aggregation of Au NPs has taken place after adding NaCl solution, which produces many SERS "hot spots" and makes the Raman reporter molecules residing in the interstitial spaces between two or more interacting particles, leading to the enormous enhancement of Raman scattering. Then, the present strategy was used for the detection of DNA. The DNA probe (see Supplementary Materials, Table S1) was first incubated with the DNA target at 37 °C for 1 h, followed by incubation with Au NPs and CV at room temperature for 30 min. After adding the NaCl solution, the surface-enhanced Raman and absorption spectra were recorded. As shown in Fig. 1A, no noticeable SERS signal was observed when incubated with the non-complementary DNA target (curve c), and the absorption spectrum as well as the color did not change compared with the monodispersed Au NPs (curve c of Fig. 1B). This implies that the ssDNA (including DNA probe and non-

complementary DNA target) can protect the Au NPs from salt-induced aggregation, showing a weak SERS signal. In contrast, when incubated with the complementary DNA target, significantly enhanced SERS signal was observed (curve d of Fig. 1A), accompanied with an obvious red-to-purple color change and appreciable absorption spectral alteration (curve d of Fig. 1B), indicating that the aggregation of Au NPs has taken place due to lack of the ssDNA protection resulting from the hybridization of DNA probe with complementary DNA target. The signal-to-background ratio between the complementary and the non-complementary DNA target was as high as ~25 (calculated by the peak area at 1612 cm^{-1}). This was attributed to the aggregation the Au NPs, which produces many "hot spots" and leads to enormous Raman enhancement factors on the order of 10^{14}–10^{15}.

Transmission electron microscopy (TEM) investigation was also performed to further verify the difference of ssDNA and dsDNA in the protection of Au NPs from salt-induced aggregation. As shown in Fig. 1C, the TEM image of the Au NPs in the presence of ssDNA protection (that is, incubated with the non-complementary DNA target) showed a majority of dispersed particles together with a minority of small aggregates. In contrast, in the absence of ssDNA protection (that is, incubated with the complementary DNA target), large Au NP aggregates of a few hundred nanometers to micrometers in diameter were observed. This gave the direct evidence for the aggregation of Au NPs, and such aggregation facilitated the formation of SERS "hot spots" and the enhancement of SERS signal.

3.2. Effect of Au NP size, CV concentration and NaCl concentration

To maximize the contrast between the "off-state" (single particles without plasmonic coupling) and "on-state" (NP aggregates with plasmonic coupling), several parameters were optimized. The Au NP size was first investigated. The monodispersed colloidal Au NP suspensions in three different particle sizes (~13, 30 and 60 nm diameter) were, respectively, synthesized by changing the sodium citrate concentration. The surface-enhanced Raman spectra of these Au NP suspensions adsorbed with CV before and after the salt-induced aggregation were recorded, and the peak area at 1612 cm^{-1} was calculated. It can be seen from Fig. S1 in Supplementary Materials that the Au NPs with 60 nm diameter can give slightly increased on/off SERS intensity ratio (that is, the contrast from single particles to NP aggregates, ~30) compared with that of Au NPs with 30 nm diameter (~25). However, we found that it was difficult to protect the 60 nm Au NPs from salt-induced aggregation using the present ssDNA even at a very high concentration. Presumably, a longer ssDNA was needed to protect the Au NPs with larger sizes from salt-induced aggregation. So, the Au NP with ~30 nm diameter was selected because it not only gave the relatively high on/off SERS intensity ratio but also can be protected well by the present ssDNA against salt-induced aggregation. In addition, CV concentration was also investigated (Fig. S2 in Supplementary Materials). In contrast to the SERS tags reported previously (Qian et al., 2008a), in which the surface of Au NPs was fully covered with the Raman reporter molecules to obtain a maximal SERS signal of single nanoparticle, the surface coverage of ~400 reporter molecules per 30 nm Au NP (approximately one-tenth of the full surface coverage) was found to be optimal in the present work. This reduction was mainly based on two reasons. First, the high surface coverage of reporter molecule made the nanoparticles difficult to be protected well by the ssDNA and prone to aggregation when negatively charged DNA was introduced. Second, by lowering the number of reporter molecules, SERS signal from single nanoparticles (off-state) was minimized relative to that from aggregated particles (on-state). Finally, it was also important to optimize the NaCl concentration. A relatively high salt concentration maybe resulted in the aggregation of the Au NPs protected by ssDNA, displaying a high background SERS signal (off-state signal from single particles), while a relatively low salt concentration cannot induce a sufficient aggregation of Au NPs, giving a low SERS signal (on-state signal from NP aggregates). It can be seen from Fig. S3 in Supplementary Materials that the maximum SERS intensity ratio (~25) was achieved when 35 mM NaCl concentration was used. In addition, the hybridization time was also optimized (Fig. S4 in Supplementary Materials) and a hybridization time of 1 h was used. The total assay time was about 1.5 h, which was faster than most methods previously reported. (Graham et al., 2008; Qian et al., 2008b; Han et al., 2010).

3.3. SERS-based detection of DNA

To verify the ability of our approach for quantitative analysis, we next performed a series of experiments at different concentrations of the complementary DNA target under the optimal experimental conditions. Fig. 2 shows the SERS spectra between 1400 and 1800 cm^{-1} at various concentrations of DNA target from 0 to 300 nM. As expected, the intensity of the Raman peak increases concomitantly with the increasing concentration of the DNA target (Fig. 2A), indicating that, with the increase in the DNA target concentration, more and more DNA probe is hybridized to form a double-stranded structure, which results in more and more Au NP aggregates due to lack of the ssDNA protection. The

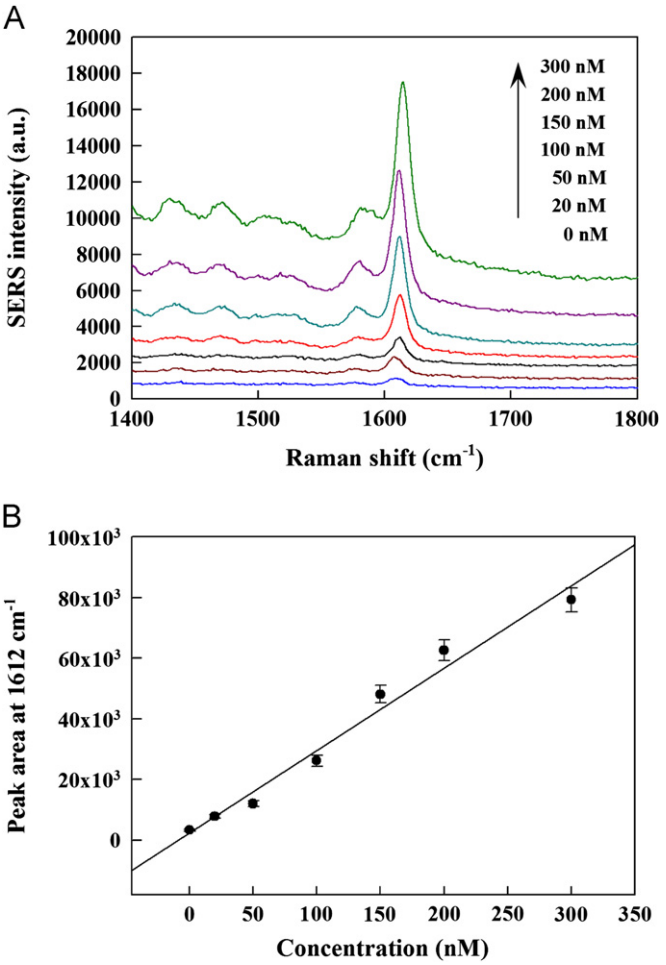

Fig. 2. (A) SERS spectra in the presence of different concentrations of complementary target DNA, and (B) plot of peak area at 1612 cm^{-1} as a function of target DNA concentration.

concentration response was quantified by observing the change in the area of the SERS peak at 1612 cm^{-1}. The results were plotted in Fig. 2B. As can be seen, a linear correlation was obtained in the concentration range from 0 to 300 nM. The detection limit was estimated to be 10 nM in terms of the rule of three times standard deviation over the blank response. Additionally, the absorption spectra at various concentrations of DNA target have also been recorded and the plot of A_{700}/A_{530} as a function of target DNA concentration is shown in Fig. S5 of Supplementary Materials. Although the sensitivity of the SERS-based approach was not remarkably superior to that of method based on UV–vis, the former possesses the excellent signal-to-background ratio as high as ~25 and can avoid effectively endogenous color interferences from the target analyte.

3.4. Discrimination of mismatched DNA

The proposed SERS-based DNA sensing method also shows good sequence specificity and is able to discriminate single-base and two-base mismatches with high SERS intensity ratio. As depicted in Fig. 3, in the presence of the DNA target with single-base A/G mutation or two-base A/G mutations, the SERS intensity decreases remarkably compared with that of perfectly matched DNA target, and the SERS intensity ratios between the perfectly matched DNA target and the mismatched DNA target are approximate three and six for single-base and two-base mismatched DNA target, respectively. This discrimination ability mainly arises from the differences in hybridization efficiency or thermal stability resulting from base mismatch. A higher SERS intensity ratio for improved discrimination ability of base mismatch can be obtained by using enzyme-aided allele discrimination, such as DNA polymerase and DNA ligase previously reported by our group (Huang et al., 2009; Li et al., 2010).

3.5. SERS-based detection of Hg^{2+}

To demonstrate the generality of this strategy, we used the same principle to develop a label-free, SERS-based biosensing technique for the detection of Hg^{2+} using unmodified Au NPs. The schematic illustration was shown in Scheme S1. The Hg^{2+} probe contains two parts: the thymine-rich mercury-binding sequence and the linker sequence (Table S1 in Supplementary Materials). In the presence of Hg^{2+}, mercury-mediated base pairs (T–Hg^{2+}–T) can be formed between thymine residues from two Hg-binding sequences to give rise to a hairpin structure. After the addition of unmodified Au NPs, Raman reporter molecules and NaCl, the aggregation of Au NPs occurs due to lack of the protection of ssDNA, resulting in a strong SERS signal. In contrast, in the absence of Hg^{2+}, the strong electrostatic attraction of ssDNA with citrate-coated Au NPs prevents the nanoparticles from salt-induced aggregation, giving a weak SERS signal. Fig. 4 showed the SERS spectra of the mixture solution of Au NPs, CV and Hg^{2+} probe in the absence and presence of 4.0 μM Hg^{2+}. As expected, in the absence of Hg^{2+}, no obvious SERS signal was observed (curve a), indicating that the Hg^{2+} probe exists in the single-stranded form and adsorbs on the surface of Au NPs to protect the Au NPs from salt-induced aggregation. A well-defined surface plasmon resonance peak at 530 nm (Fig. S6A in Supplementary Materials) also implied the monodispersed state of the Au NPs. While in the presence of Hg^{2+}, the SERS spectrum was dramatically turned on by strong plasmonic coupling and electromagnetic enhancement, and this coupling also resulted in significant broadening and red shifting of the absorption spectrum (Fig. S6A in Supplementary Materials). These results suggest that binding of Hg^{2+} with probe forms a double-stranded structure, which reduces the interaction with Au NPs and leads to the Au NP aggregation and the enhancement of SERS signal. This aggregation was also demonstrated by the TEM images of Au NPs in the presence of Hg^{2+} (Fig. S6B in Supplementary Materials). The SERS signal-to-background ratio (represented by the peak area at 1612 cm^{-1}) was as high as ~35 under the optimal experimental conditions selected in the DNA detection.

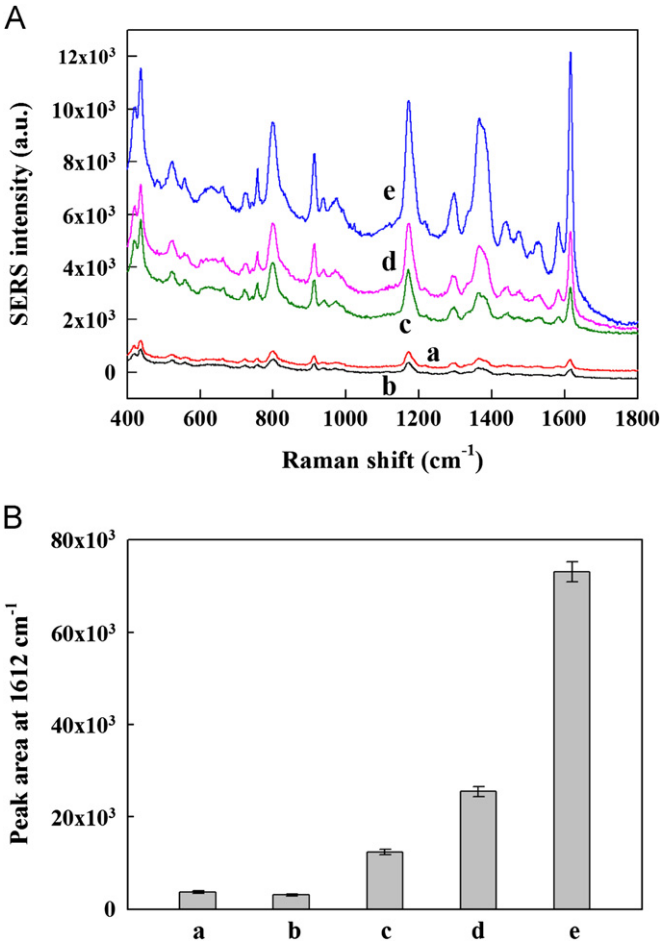

Fig. 3. (A) SERS spectra in the absence of DNA target (a), in the presence of non-complementary DNA target (b), two-base mismatched DNA target (c), single-base mismatched DNA target (d), and complementary DNA target (e). The DNA target concentration was 200 nM. (B) The corresponding histogram represented with the peak area at 1612 cm^{-1}. The DNA sequences were shown in Supplementary Materials, Table S1.

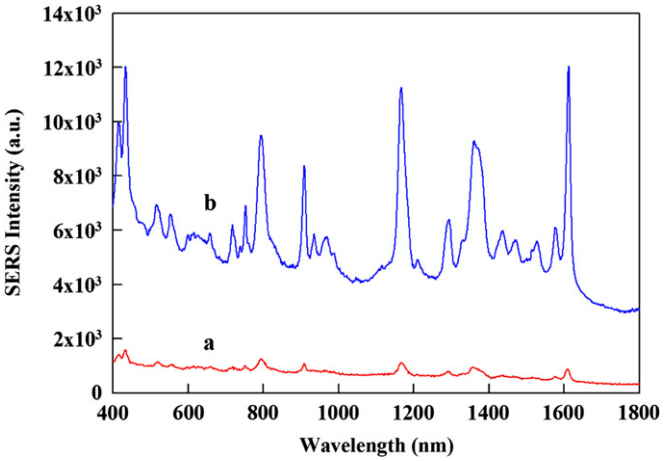

Fig. 4. SERS spectra of the mixture solution of Au NPs, CV and Hg^{2+} probe in the absence (a) and presence (b) of 4.0 μM Hg^{2+} after adding 35 mM NaCl.

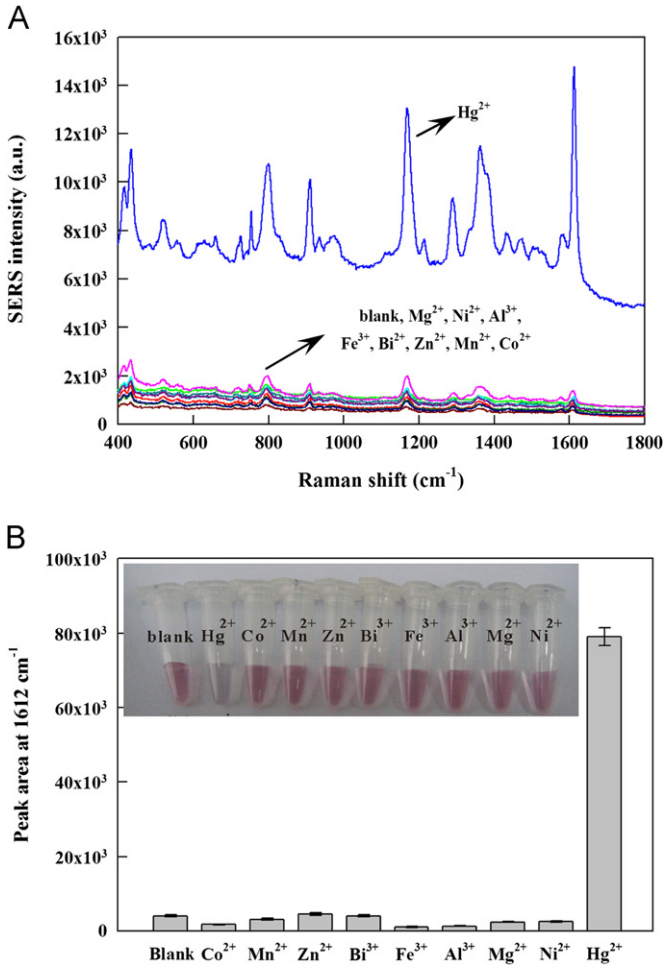

Fig. 5. Selectivity of SERS-based Hg^{2+} sensing technique. (A) SERS spectra in response to 4.0 μM Hg^{2+} and 40.0 μM of other metal ions. (B) The corresponding histogram represented with the peak area at 1612 cm^{-1}. The inset is the photograph for the corresponding systems.

Next, the SERS spectra between 1400 and 1800 cm^{-1} at various concentrations of Hg^{2+} ion from 0 to 3.0 μM were investigated. The intensity of the Raman peak increased concomitantly with the increasing Hg^{2+} concentration, and a linear correlation between the peak area at 1612 cm^{-1} and Hg^{2+} concentration was obtained in the concentration range from 0 to 3.0 μM (Fig. S7 in Supplementary Materials). The detection limit for Hg^{2+} was estimated to be 0.2 μM in terms of the rule of three times standard deviation over the blank response. A higher Hg^{2+} concentration above 3.0 μM did not give rise to a stronger SERS signal. Also, the absorption spectra at various Hg^{2+} concentrations have also been recorded and the plot of A_{700}/A_{530} as a function of Hg^{2+} concentration is shown in Fig. S8 of Supplementary Materials. Although the sensitivity of the SERS-based approach was not remarkably superior to that of method based on UV–vis, the former possesses the excellent signal-to-background ratio as high as ~30 and can avoid effectively endogenous color interferences from the target analyte. Finally, the selectivity of the proposed technique for the detection of Hg^{2+} was also investigated. Fig. 5A illustrated the SERS spectra in response to 4.0 μM Hg^{2+} and 40.0 μM of other metal ions. An intense SERS signal was observed for Hg^{2+} solution, while all other metal ions could not induce any detectable SERS signal even at a concentration 10 times higher than that of Hg^{2+}. Fig. 5B was the corresponding histogram represented with the peak area at 1612 cm^{-1}. The high SERS intensity ratios (~30–40) between Hg^{2+} and other metal ions exhibits excellent selectivity of our proposed technique to Hg^{2+} over other competing metal ions, which indicates that the proposed sensor can meet the real sample detection and can be applied to the Hg^{2+} detection in environmental and biological fields.

4. Conclusions

We have developed a label-free, homogeneous and easy-to-operate biosensing platform for the rapid, simple and sensitive SERS detection using unmodified Au NPs. This strategy utilizes the difference in adsorption property of ssDNA and dsDNA on citrate-coated Au NPs, which leads to the difference in the protection of Au NPs against salt-induced aggregation, as well as the fact that the aggregation of monodispersed Au NPs can give rise to the plasmonic coupling and turn on the enhancement of the Raman scattering. This approach is not only straightforward and simple in design, but also fairly rapid and convenient in operation. Furthermore, in contrast to the methods based on SERS tags which require the covalent modification of the metallic nanoparticles with the Raman active dye and biorecognition element, the proposed strategy employs unmodified Au NPs, which circumvents the time-consuming and complicated covalent modification process and significantly simplifies the procedure of SERS detection. Herein, we have demonstrated successfully the application of this strategy in the detection of DNA and Hg^{2+}, and the assay possesses the superior signal-to-background ratio as high as ~30 and excellent selectivity. Factually, this method can in principle be extended to detect various analytes, such as other metal ions, proteins and small molecules by using the oligonucleotides that can selectively bind the analytes. This work offers a new approach of using unmodified Au NPs for label-free, sensitive and selective SERS-based biosensing.

Acknowledgments

This work was supported by the National Natural Science Foundation of China (No. 20975035, 21275045), NCET-11–0121, and Hunan Provincial Natural Science Foundation of China (Grant 12JJ1004).

Appendix A. Supporting information

Supplementary data associated with this article can be found in the online version at http://dx.doi.org/10.1016/j.bios.2012.12.002.

References

Braun, G., Lee, S.J., Dante, M., Nguyen, T.-Q., Moskovits, M., Reich, N., 2007. Journal of the American Chemical Society 129, 6378–6379.
Campion, A., Kambhampati, P., 1998. Chemical Society Reviews 27, 241–250.
Cantor, C.R., Warshaw, M.M., Shapiro, H., 1970. Biopolymers 9, 1059–1077.
Cao, Y.C., Jin, R., Mirkin, C.A., 2002. Science 297, 1536–1540.
Chon, H., Lim, C., Ha, S.-M., Ahn, Y., Lee, E.K., Chang, S.-I., Seong, G.H., Choo, J., 2010. Analytical Chemistry 82, 5290–5295.
Darbha, G.K., Singh, A.K., Rai, U.S., Yu, E., Yu, H., Ray, P.C., 2008. Journal of the American Chemical Society 130, 8038–8043.
Graham, D., Thompson, D.G., Smith, W.E., Faulds, K., 2008. Nature Nanotechnology 3, 548–551.
Griffin, J., Singh, A.K., Senapati, D., Lee, E., Gaylor, K., Jones-Boone, J., Ray, P.C., 2009. Small 5, 839–845.
Han, X.X., Chen, L., Guo, J., Zhao, B., Ozaki, Y., 2010. Analytical Chemistry 82, 4102–4106.
Han, X.X., Huang, G.G., Zhao, B., Ozaki, Y., 2009a. Analytical Chemistry 81, 3329–3333.
Han, X.X., Kitahama, Y., Itoh, T., Wang, C.X., Zhao, B., Ozaki, Y., 2009b. Analytical Chemistry 81, 3350–3355.

Han, X.X., Jia, H.Y., Wang, Y.F., Lu, Z.C., Wang, C.X., Xu, W.Q., Zhao, B., Ozaki, Y., 2008. Analytical Chemistry 80, 2799–2804.
Hao, E., Schatz, G.C., 2004. The Journal of Chemical Physics 120, 357–366.
He, L., Rodda, T., Haynes, C.L., Deschaines, T., Strother, T., Diez-Gonzalez, F., Labuza, T.P., 2011. Analytical Chemistry 83, 1510–1513.
Herne, T.M., Ahern, A.M., Garrell, R.L., 1991. Journal of the American Chemical Society 113, 846–854.
Huang, Y., Zhang, Y.L., Xu, X., Jiang, J.H., Shen, G.L., Yu, R.Q., 2009. Journal of the American Chemical Society 131, 2478–2480.
Hwang, H., Chon, H., Choo, J., Park, J.-K., 2010. Analytical Chemistry 82, 7603–7610.
Jarvis, R.M., Brooker, A., Goodacre, R., 2004. Analytical Chemistry 76, 5198–5202.
Kahraman, M., Sur, I., Culha, M., 2010. Analytical Chemistry 82, 7596–7602.
Lee, J.H., Wang, Z., Liu, J., Lu, Y., 2008. Journal of the American Chemical Society 130, 14217–14226.
Li, H., Rothberg, L.J., 2004a. Proceedings of the National Academy of Sciences of the United States of America 101, 14036–14039.
Li, H., Rothberg, L.J., 2004b. Journal of the American Chemical Society 126, 10958–10961.
Li, J., Deng, T., Chu, X., Yang, R., Jiang, J.H., Shen, G.L., Yu, R.Q., 2010. Analytical Chemistry 82, 2811–2816.
Li, M., Zhang, J., Suri, S., Sooter, L.J., Ma, D., Wu, N., 2012. Analytical Chemistry 84, 2837–2842.
Lierop, D., Faulds, K., Graham, D., 2011. Analytical Chemistry 83, 5817–5821.
Liu, X., Knauer, M., Ivleva, N.P., Niessner, R., Haisch, C., 2010. Analytical Chemistry 82, 441–446.
Lowe, A.J., Huh, Y.S., Strickland, A.D., Erickson, D., Batt, C.A., 2010. Analytical Chemistry 82, 5810–5814.
Michaels, A.M., Nirmal, M., Brus, L.E., 1999. Journal of the American Chemical Society 121, 9932–9939.
Mitchell, B.L., Patwardhan, A.J., Ngola, S.M., Chan, S., Sundararajan, N., 2008. Journal of Raman Spectroscopy 39, 380–388.
Nie, S., Emory, S.R., 1997. Science 275, 1102–1106.
Ock, K., Jeon, W.I., Ganbold, O., Kim, M., Park, J., Seo, J.H., Cho, K., Joo, S.-W., Lee, S.Y., 2012. Analytical Chemistry 84, 2172–2178.
Preciado-Flores, S., Wheeler, D.A., Tran, T.M., Tanaka, Z., Jiang, C., Barboza-Flores, M., Qian, F., Li, Y., Chen, B., Zhang, J.Z., 2011. Chemical Communications, 4129–4131.
Qian, X., Li, J., Nie, S., 2009. Journal of the American Chemical Society 131, 7540–7541.
Qian, X., Peng, X.H., Ansari, D.O., Yin-Goen, Q., Chen, G.Z., Shin, D.M., Yang, L., Young, A.N., Wang, M.D., Nie, S., 2008a. Nature Biotechnology 26, 83–90.
Qian, X., Zhou, X., Nie, S., 2008b. Journal of the American Chemical Society 130, 14934–14935.
Ray, P.C., 2006. Angewandte Chemie-International Edition 45, 1151–1154.
Schmit, V.L., Martoglio, R., Carron, K.T., 2012. Analytical Chemistry 84, 4233–4236.
Tang, H.W., Yang, X.B.B., Kirkham, J., Smith, D.A., 2008. Applied Spectroscopy 62, 1060–1069.
Wang, G., Lipert, R.J., Jain, M., Kaur, S., Chakraboty, S., Torres, M.P., Batra, K., Brand, R.E., Porter, M.D., 2011. Analytical Chemistry 83, 2554–2561.
Wang, H., Wang, Y., Jin, J., Yang, R., 2008a. Analytical Chemistry 80, 9021–9028.
Wang, Z., Lee, J.H., Lu, Y., 2008b. Advanced Materials 20, 3263–3267.
Wang, Z., Pan, S., Krauss, T.D., Du, H., Rothberg, L.J., 2003. Proceedings of the National Academy of Sciences of the United States of America 100, 8638–8643.
Wei, H., Li, B., Li, J., Wang, E., Dong, S., 2007. Chemical Communications, 3735–3737.
Xin, A., Dong, Q., Xiong, C., Ling, L., 2009. Chemical Communications, 1658–1660.
Yang, X., Gu, C., Qian, F., Li, Y., Zhang, J.Z., 2011. Analytical Chemistry 83, 5888–5894.
Zhang, H., Harpster, M.H., Park, H.J., Johnson, P.A., Wilson, W.C., 2011. Analytical Chemistry 83, 254–260.
Zhang, J., Wang, L., Pan, D., Song, S., Boey, F.Y.C., Zhang, H., Fan, C., 2008. Small 4, 1196–1200.
Zong, S., Wang, Z., Yang, J., Cui, Y., 2011. Analytical Chemistry 83, 4178–4183.